Miriam Simon, Albert Prause, Albert Prause, Michael Gradzielski

Self-assembled single-stranded DNA nano-networks in solution and at surfaces

Self-Assembled ssDNA Nano-networks in Solution and at Surfaces

Miriam Simon[1,2,3*], Albert Prause[1], Stefan Zauscher[3*], Michael Gradzielski[1*]

1: Stranski-Laboratorium für Physikalische und Theoretische Chemie, Institut für Chemie, Technische Universität Berlin, D-10623 Berlin, Germany

2: Duke University, Department of Material Engineering and Material Science, Durham, North Carolina, USA

3: Dept. of Chemical Engineering and the Russell Berrie Nanotechnolgy Inst. (RBNI), Technion-Israel Institute of Technology, Haifa, IL-3200003, Israel

*miriam.simon@campus.technion.ac.il

*zauscher@duke.edu

*michael.gradzielski@tu-berlin.de

ABSTRACT

We studied the directed self-assembly of two types of complementary ssDNA strands (i.e., poly(dA) and poly(dT)) into more complex, organized and percolating networks in dilute solution and at surfaces. Understanding ssDNA self-assembly into 2D-networks on surfaces is important for the use of such networks in the fabrication of well-defined nanotechnological devices, as for instance required in nanoelectronics or for biosensing. To control the formation of 2D-networks on surfaces it is important to know whether DNA assemblies are formed already in dilute solution or only during the drying/immobilization process at the surface, where the concentration automatically increases. Fluorescence Cross-Correlation Spectroscopy (FCCS) clearly shows the presence of larger DNA complexes in mixed poly(dA) and poly(dT) solutions already at very low DNA concentrations (<1 nM); i.e., well below the overlap concentration. Here, we describe for the first time, such supramolecular complexes in solution and how their structure depends on the ssDNA length, concentration, and ionic strength. Hence, future attempts to control such networks should also focus on its state in solution and not only on its immobilization on surfaces.

KEYWORDS

ssDNA, assembly, fluorescence cross-correlation spectroscopy, networks, bionanotechnology

INTRODUCTION

One of the main challenges for bionanotechnology still is to develop strategies that overcome some of the current scaling-limitations in DNA (deoxyribonucleic acid) nanofabrication, especially for creating well-defined polynucleotide networks on surfaces. Access to such DNA networks over macroscopic areas would advance the field, because such networks address an essential need for the fabrication of nanoscale devices with applications ranging from optoelectronics, sensing, flexible electronics, to photovoltaics.[1,2] A single-stranded DNA chain has a width of only ~1 nm and can be synthesized with precisely controllable lengths ranging from the nanometer to the millimeter length scale.[3,4] Access to this range of dimensions combined with other desirable properties, such as DNA's molecular recognition properties, versatile ways of manipulation,[5] and the easy synthesis via enzymatic polymerization,[4,6] make ssDNA an exciting material for nanofabrication,[7–10] including tailored surface engineering.[11] As such, DNA provides a natural template for nanofabrication and molecular nanotechnology,[12,13] where DNA has been successfully employed to organize nanoparticles into arrays via base pairing,[14,15] and as linear template for the fabrication of metallic, magnetic or semiconducting nanowires.[16–18]

For most practical applications the nanosized templates have to be immobilized on a surface.[19] Consequently, there is a substantial body of work that deals with the controlled deposition, orientation and alignment of DNA structures on surfaces.[20–24] For example, DNA-based multilayers have been obtained by alternatively depositing complementary, single stranded poly(dA/dG) and poly(dT/dC).[25] To obtain ordered networks with defined connectivity, more complicated, multi-step processes have to be used.[26] It is, however, possible to form large-scale DNA networks through the self-assembly of two complementary ssDNA strands in solution and depositing the resulting structure onto a surface.[27] This has also been shown for the case of rather short (50 bp) mixtures of poly(dA) and poly(dT) to lead to networks of 100-200 nm mesh size[28], where this process subsequently was also described by coarse-grained Molecular Dynamics (MD).[29] In a related fashion one may start by dropping a DNA solution onto a mica surface, where subsequent drying also leads to the formation of DNA networks, provided a sufficiently high concentration

of Mg^{2+} (> 1 mM) is employed in the process. Mg^{2+} induces attractive interactions between the negatively charged DNA and the negatively charged mica surface.[30]

While the mechanism of surface-mediated DNA hybridization[31] and the hybridization kinetics, determined by single-molecule fluorescence imaging on a glass surface, are known,[32] much less is known about the formation of self-assembled DNA network structures in solution. Some investigations in this area have focused on building up larger scale, space-filling structures, like the formation of DNA hydrogels,[33] but investigations about DNA self-assembly in dilute solutions, as they are used for surface deposition, and how this process depends on the concentration and length of individual strands, and the ionic strength of the suspension medium are lacking. On one hand, self-assembly is favored due to base pairing, but one the other hand this has to occur against the electrostatic repulsion of the equally charged polyelectrolyte chains. We surmise that the dilute solution state greatly influences the surface deposition process and the resulting ssDNA network structures.

Here, we report on our research aimed at preparing well-defined ssDNA networks on surfaces and over large areas by self-assembly, and how this process is related to the structures present in dilute solution. Specifically, we were interested in understanding the parameters that control ssDNA self-assembly in solution and how the resulting structures can be transferred onto a surface, thereby delivering the design rules for the fabrication of well-defined DNA network nanostructures. Our experiments, using fluorescence cross-correlation spectroscopy (FCCS), show that aggregation of the ssDNA leads to larger structural units already at very low solution concentrations (sub-nM regime, *i.e.*, well below the overlap concentration) and thus affect the formation of 2D networks on surfaces.

EXPERIMENTAL

Materials

ss-poly(dA) and ss-poly(dT) strands were synthesized separately by TdT-catalyzed, enzymatic polymerization (TcEP), using fluorescently labeled oligonucleotides as initiators and the template

independent enzyme terminal deoxynucleotidyl transferase (TdT).[4] TdT sequentially adds monomers to the terminal 3'-OH-group of the initiators. For the synthesis the initiator, the monomer (here dATP or dTTP) and TdT were mixed in a TdT-buffer/H_2O solution. The oligonucleotide initiators (Cy5-dA and Alexa488-dT) were purchased from Integrated DNA Technologies, Inc. (Coralville, IA). TdT enzyme, TdT buffer, and natural dNTP monomers were purchased from Promega (Madison, WI). The total reaction volume was set to 100 µL. The monomer-to-initiator ratio (*M/I*) determines the resulting polymer chain length (molecular weight, M_W) and can be adjusted accordingly.[6] Furthermore, we previously showed that resulting molecular weight distributions are narrow (i.e., Poisson distributed), approaching a polydispersity index (PDI = M_w/M_n) of 1.0.[6] Polymerizations were carried out at 37 °C for two hours before termination by heating the mixture up to 70 °C for 10 minutes. The products were purified by centrifugal filtration in columns (Microcon YM-30 centrifugal filter device, Millipore). Using this approach, we synthesized nearly monodisperse, single stranded polynucleotides with different M_Ws. The M_Ws of the reaction products were determined by gel electrophoresis (C.B.S Scientific Company, Inc). To determine the M_W of the ssDNA we constructed a M_W ladder from standard polynucleotides (Invitrogen, CA) and used the fluorophores in the initiators of the ssDNA chains to visualize the polymers in the gel, using a Typhoon 9410 fluorescence scanner (GE Healthcare Life Science, Piscataway, NJ), see SI for a representative gel image. The solution concentrations were determined by comparing the measured concertation of the fluorescent dyes contained in the initiators (Nanodrop fluorimeter, Thermo Scientific) to a previously established calibration curve. Specifically, we synthesized Alexa488 labeled ss-poly(dT) strands of 1300 B length and Cy5 labeled ss-poly(dA) strands of 50, 500, 1000 and 8000 B length. Cy5 has an absorbance maximum at 648 nm and the fluorescence emission maximum is at 668 nm, whereas Alexa488 absorbs light of 488 nm and emits at 520 nm.

Methods

Atomic Force Microscopy (AFM)

All AFM measurements were carried out in air and at room temperature with a MultiMode AFM (Bruker), using TappingMode silicon cantilevers (k_F = 40 N/m, f_{res} = 311 – 357 kHz, R_{Tip} < 10 nm, Bruker).

Fluorescence (Cross-)Correlation Spectroscopy (FCS/FCCS)

FCS/FCCS measurements were performed on a Leica TCS SP5 II confocal microscope with a Picoquant FCS setup. Continuous Ar (λ = 488 nm) and HeNe (λ = 633 nm) lasers were used as light sources. The light was delivered at the sample through an apochromatic 63x, 1.2 NA water immersion objective and the fluorescence light was collected through the same objective. Both fluorophores were excited simultaneously with the two lasers and a 500-550/647-703 nm beamsplitter was used to separate the emitted light of the two different dyes. In this way, auto-correlation functions can be calculated of each dye separately and, more interestingly, a cross-correlation function of both dyes can be calculated. The latter is only considering the movements of both dyes together, indicating that they are bound together, for instance in a complex or network. The measured data for the auto-correlation functions were fitted with:

$$G(\tau) = \frac{1}{\langle N \rangle} \int P(x, \tau_D, \sigma_D) \cdot G_D(\tau, x)\, \mathrm{d}x, \tag{1}$$

where $\langle N \rangle$ is the average number of fluorescent molecules in the confocal volume, $P(x, \tau_D, \sigma_D)$ the lognormal distribution with τ_D as median of the diffusion time and σ_D as standard deviation (log-space) written as:

$$P(x, \tau_D, \sigma_D) = \frac{1}{\sqrt{2\pi} \cdot \sigma_D \cdot x} \cdot \exp\left(-\frac{(\ln(x) - \ln(\tau_D))^2}{2\sigma_D^2}\right), \tag{2}$$

and $G_D(\tau, \tau_D)$ the normalized correlation function with τ as correlation time and k as anisotropy of the confocal volume:

$$G_D(\tau, \tau_D) = \left(1 + \frac{\tau}{\tau_D}\right)^{-1} \cdot \left(1 + \frac{\tau}{\tau_D \cdot k^2}\right)^{-\frac{1}{2}}. \tag{3}$$

Calibration of the confocal volume was performed using AlexaFluor488 as a reference dye with known diffusion coefficient of 435 μm²/s, at different concentrations. The anisotropy is defined as: $k = z_i/w_i$, where

z_i is the longitudinal and w_i the lateral beam radius of the confocal volume. The lateral beam radius for channel 1 (Ar laser), $\omega_{1,}$ was found to be 0.19(±0.02) µm and k was fixed to 6(±1). Thus, the effective confocal volume $V_{eff,1} = \pi^{3/2}\, w_1^3 \cdot k$ evaluates to 0.23(±0.06) fL. For channel 2, the HeNe laser, the lateral beam radius w_2 was found to be 0.22(±0.02) µm and k was held unchanged, thus the effective confocal volume $V_{eff,2}$ was 0.36(0.1) fL. For cross-correlation functions, the lateral beam radius w_{12} is averaged as $w_{12}^2 = (w_1^2 + w_2^2)/2$ and the effective confocal volume $V_{eff,2}$ was 0.29(±0.08) fL, accordingly.

The diffusion coefficient was be obtained from the decay time as follows:

$$D_{f,i} = \frac{w_i^2}{4 \cdot \tau_{D,i}}\,. \tag{4}$$

Approach

We studied the self-assembly properties of mixtures of ss-poly(dA) and ss-poly(dT) in aqueous solution and after deposition on mica surfaces. While initially we were interested in the structures formed on surfaces, we soon noticed that interesting self-assembly already takes place in very dilute solution, that might largely influence the outcome of the structure of the surface-deposited network. This experimental path is described below, starting with the preparation and characterizing of networks on the mica surface, and then studying in thorough detail the self-assembly in the bulk solutions. In our experiments we varied the mixing ratio, the length of the individual ss-poly(dA/dT) strands and their concentration, and also the ionic strength of the solutions to establish how these parameters affect the structures in bulk solution as well as on surfaces.

Bulk Solutions

Samples were prepared by first mixing ss-poly(dA) and ss-poly(dT) stock solutions in the desired ratio. The mixture was then diluted with DI water to the desired concentration. $MgCl_2$ solutions were used for dilution when desired. For studying the solution behavior by FCS, we tested three different preparation pathways: (i) first mixing concentrated stock solutions and then diluting, (ii) first diluting the stock solution before

mixing, adding salt, and (iii) letting the mixture incubate overnight (see Figure S11 for FCS data). Interestingly, the different preparation pathways did not have a noticeable effect on the emergence of final aggregates, *i.e.*, we thus conclude that thermal equilibrium conditions likely prevailed in the studied systems. We thus also assume that the surface aggregation is unaffected by the order of mixing. Since a fluorescent dye is already contained in the initiator of every DNA strand, no additional sample preparation steps were needed for FCS/FCCS measurements.

Preparation of Surface Networks

For network formation on mica surfaces (freshly cleaved mica discs, 10 mm diameter), a concentration of about 9 nM (in terms of total DNA strands) was found to be ideal in concentration dependent experiments. To enable the electrostatic binding of negatively charged DNA to the negatively charged mica surfaces, we added $MgCl_2$ (8 mM) to the sample mixture prior to drop casting. To this end we used a pipette to deposit a 6 µL drop of the DNA-$MgCl_2$ mixture onto the hydrophilic mica substrate, where it immediately spread uniformly over the whole surface area. After an incubation time of two minutes, allowing the DNA to interact with the surface, we rinsed the substrate with DI-water to remove the remaining excess salt and free DNA chains, and then dried the sample in a directed stream of dry N_2. The whole process is shown schematically in Figure 1.

In addition to drop casting, we studied several other methods (including spin coating, dip-coating, and microchannels) to deposit the solution onto a substrate surface. We found that drop casting, where the dilute sample solution is simply deposited onto a freshly cleaved mica substrate, yields the most consistent and reproducible results in terms of network formation (results shown in SI). In contrast to other reported approaches, this drop casting method provides access to large-scale (order of cm^2) and percolating DNA network structures without any special equipment.[27]

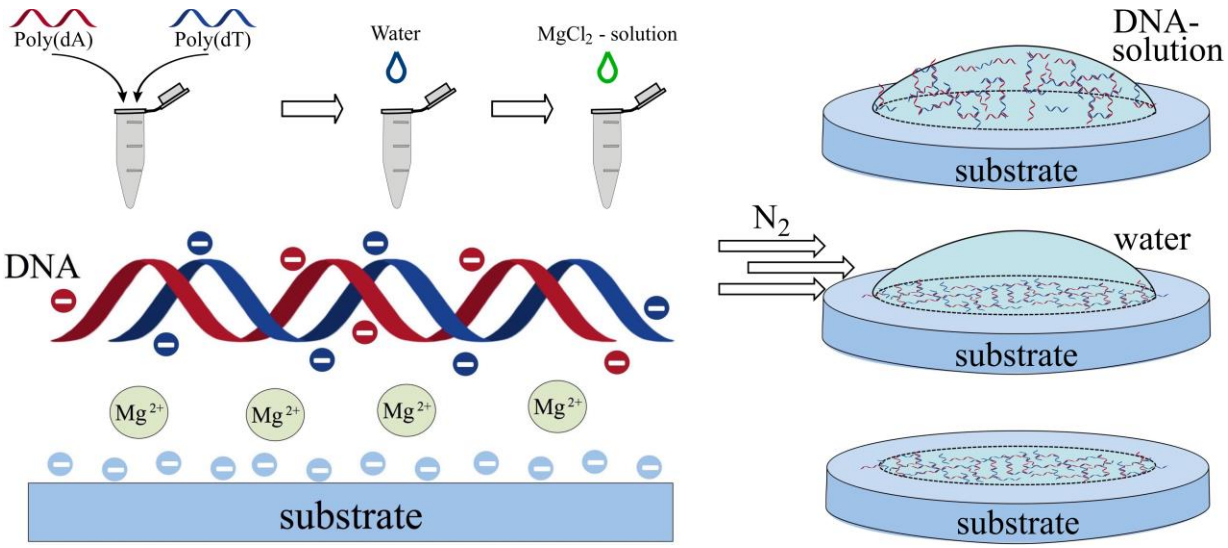

Figure 1. Schematic showing the process of preparing DNA networks on a mica substrate. First, the aqueous solution containing the desired concentration of complementary ssDNA is prepared. After deposition, binding of the DNA to the mica substrate is mediated by Mg^{2+} ions. Next, unbound DNA and salts are removed by rinsing with DI water, and finally the sample is dried in a stream of N_2.

RESULTS AND DISCUSSION

ssDNA Assembly on Surfaces

When preparing DNA assemblies on mica surfaces we observed that mixtures of complementary ss-poly(dA) and ss-poly(dT) strands can form large, percolating, and well-defined networks (Figure 2, some percolating strands are highlighted in blue). In Figure 2 one can see an interconnected 2D-network of hybridized DNA with a mesh size of 30-70 nm (estimated from the image). A concentration of 9 nM (total concentration of DNA strands) was found to be most effective for network formation, because at higher concentrations DNA multilayers formed and at lower concentrations the amount of deposited DNA was insufficient for continuous network formation (see also below).

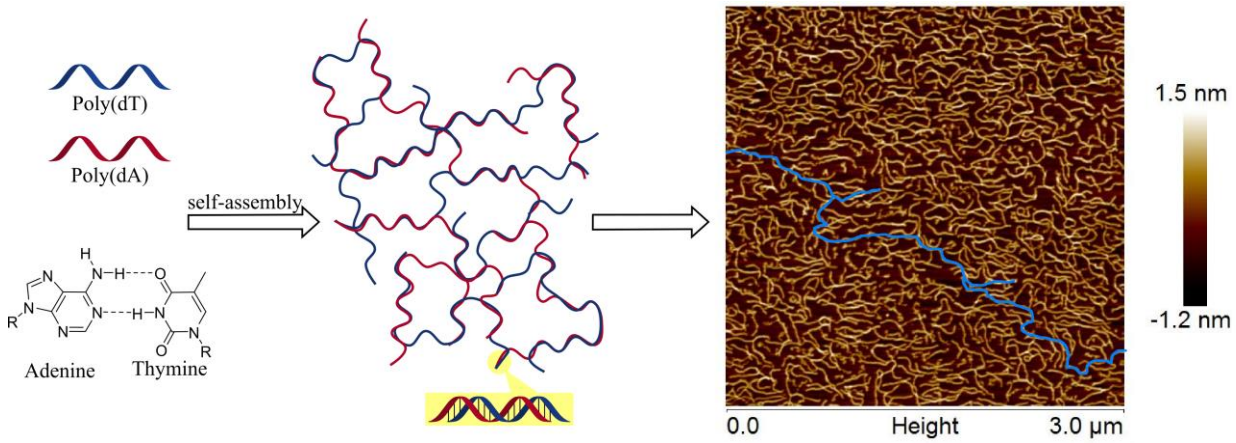

Figure 2. Schematic and AFM image of a self-assembled DNA network. The network was formed by depositing a 50:50 mixture of poly(dA) (1 kB) and poly(dT) (1.3 kB) with a total concentration of 9 nM onto a mica surface by drop casting and subsequent blow drying. poly(dA) and poly(dT) were mixed in solution prior to deposition. The blue line in the AFM image indicates a percolating pathway formed by a series of connected strands.

A ssDNA of 1000 B has a contour length of about 340 nm and therefore is much larger than the typical mesh size observed on the surfaces. We thus conclude that a single strand is likely involved in the formation of several meshes. An interesting question that arises now is whether network formation occurs already in (dilute) solution prior to deposition, or only after deposition on the surface. If the 1000 B ssDNA were fully stretched to 340 nm, then the corresponding overlap concentration c^* would be 42 nM. The other extreme would be to assume that ssDNA adopts a Gaussian coil conformation, for which an upper limit of the overlap concentration c^* would be approximately ~62 µM (calculated using l_p = 1.89 nm, [34] see SI for calculation details). A likely more realistic estimate of $c^* \approx 400$ nM can be obtained from the experimentally measured hydrodynamic radius R_h of ~ 15.5 nm (see Table 1), assuming a cylindrical geometry and applying Broersma's equation[35,36] which yields an effective cylinder length of 163 nm (assuming a diameter of 1 nm for ssDNA). We thus conclude that at our working concentration of 9 nM, ssDNA strands canno overlap. Thus, one would assume that network formation only takes place after deposition and upon evaporation of the solvent during the drying process, bringing the ssDNA concentration above the critical overlap concentration.

To address this question experimentally we prepared one sample by first drop casting single-stranded poly(dT) onto a mica substrate (2 min incubation time, washed with DI water, and dried with nitrogen) and then depositing poly(dA) onto the same surface (using the same procedure). This sequentially deposited sample only showed ssDNA (see Figure S2, SI) and no network formation. Furthermore, in none of the different deposition methods (drop casting, microchannels, spin coating, dip coating) did we observe any pronounced strand alignment (see Figure S3-5). These two observations suggest that network formation is already initiated in the solution state, prior to deposition. Accordingly, we surmise that the structures that nucleate in bulk solution largely determine the structure we observe on the substrate surface and attempts to control the networks should also take their state in solution into account. However, to date, the formation of complementary DNA networks in dilute solutions has not been examined in detail, and therefore was focused on in this study. A~~ccordingly, this became now a focus of this study.~~

Structure of ssDNA Mixtures in Solution

Our results regarding structure formation on the surface clearly suggest that ssDNA interactions in bulk solution are important for the formation of 2D-network structures at surfaces. To examine the behavior of complementary, homopolynucleotides in solution in more detail, we carried out FCS/FCCS measurements which can reveal the dynamics of polymers, even in very dilute solutions. Since we used fluorescently labeled initiator in our DNA synthesis, every single ssDNA strand was suitably labeled for FCS measurements. Specifically, we first used Cy5-labeled poly(dA) and Alexa488-labeled poly(dT) strands of similar length, *i.e.*, 1000 and 1300 bases, respectively. Using two different dyes allowed us to monitor the two ssDNA polymers separately and determine their movement together via dual color-FCCS.

First, we carried out FCS measurements on single stranded poly(dA) and poly(dT) separately. Both samples showed a characteristic decay in their correlation functions that can directly be converted into a diffusion coefficient D_f and an effective hydrodynamic radius R_h, which are 16.2(±3.3) nm and 14.9(±3.3) nm for ss-poly(dA) and ss-poly(dT), respectively (Figure 3 and Table 1). When comparing the two ssDNA, we basically see identical behavior and accordingly quite similar hydrodynamic radii for both

ssDNA types (note the different effective confocal volumes for red and blue laser, which cause slightly different radii, even though the correlation functions appear very similar in the graph, see also the Methods section for more details). The somewhat higher R_h value for poly(dA), despite its somewhat shorter length, agrees with previous observations by SAXS that poly(dA) is always stiffer than poly(dT).[37] The poly(dT) measurements in Figure 3 show a very small tailing towards longer correlation times, possibly arising from dimer formation.[38] Therefore we fitted the data with a bimodal model (only the main contribution is reported in Table 1 to avoid confusion, more details can be found in the SI). A similar behavior is absent in the poly(dA) measurements. As discussed above, the experimental value for R_h corresponds to a rigid cylinder of ~ 163 nm in length and 1 nm in diameter. This dimension is much shorter than the contour length of 340 nm for a ssDNA with 1000 B. Accordingly, we conclude that the ssDNA here is somewhat coiled in solution, in good agreement also with recent work focused on describing the structure of ssRNA in aqueous solution by SAXS experiments.[39]

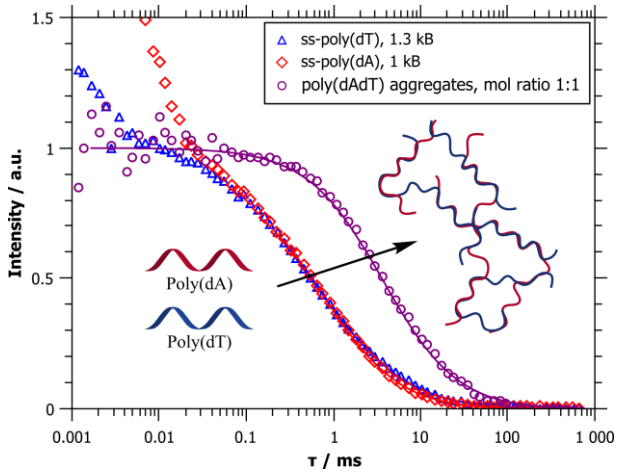

Figure 3. Auto-correlation functions of free ssDNA and cross-correlation function of the mixed sample, showing that self-assembly into larger structures takes place in solution already well below the overlap concentration. All intercepts were normalized to 1 for better comparison. Solid lines are best fits, all parameters are given in the SI and Table 1.

Next, we mixed two complementary ssDNA strands of similar lengths (1000 and 1300 bases) in a 1:1 mixing ratio, to reach a final total concentration of 9 nM, and we studied the mixture by FCS. In these experiments, we excited the two different dyes simultaneously with two different lasers (Ar 488 nm and HeNe 633 nm) and measured the fluorescence intensity after passing through a dual band-pass filter (500-550/647-703 nm). This method allowed us to calculate the auto- and cross-correlation functions of both dyes, where the latter only accounts for the movement of both dyes together (Figure 3).[40]

The existence of a cross-correlation function implies that both dyes move together through the confocal volume which suggests that the complementary poly(dA) and poly(dT) strands are bound together in larger aggregates or networks. The comparison of the cross-correlation function of the mixed sample with the auto-correlation functions of the free ssDNA shows a much slower decay of the cross-correlation function. This suggests that much larger aggregates (R_h = 85.4(±17.1) nm) are formed that consist of several single strands hybridized to dsDNA within even larger AT structures (R_h of free ssDNA ~15.5 nm; Table 1).

Table 1. Diffusion coefficients (D_f) and hydrodynamic radii (R_h) derived from FCS/FCCS measurements (c = 9 nM). Standard deviations ($\pm\sigma_D$) are given in parentheses. (It should be noted that the absolute value of R_h is not very precise in FCS/FCCS (see given error bars), mainly due to the experimental uncertainty in the confocal volume, but the relative changes in size are much more precise)

	D_f / µm²/s	R_h / nm
ss-poly(dA) (1 kB)	15.1(±3.1)	16.2(±3.3)
ss-poly(dT) (1.3 kB)	16.4(±3.6)	14.9(±3.3)
poly(dAdT) aggregates	2.87(±0.6)	85.4(±17.1)

The R_h values measured for poly(dAdT) aggregates are, however, too small to account for the large-scale networks we observed on the surfaces by AFM imaging. There are two possibilities to explain this discrepancy, either only smaller aggregates are formed and observed in solution, or the FCS measurements only show segmental diffusion of the network, due to the small confocal volume and the dynamic nature of such a network. However, at the concentrations studied here, ssDNA cannot form a space filling network,

because even if we consider a maximum length of 340 nm for the 1 kB ssDNA, *i.e.*, completely stretched chains, the overlap concentration would still only be 42 nM, a concentration that is larger than that used in the experiments. In reality, ssDNA (R_h ~ 15.5 nm) is much more likely to behave like a flexible rod, and as discussed above, the overlap concentration in that case would be even higher (~ 400 nM). Accordingly, no fully space-filling network can be formed in solution. This suggests that only poly(dAdT) aggregates of mixed ssDNA with R_h of 85 nm are formed, that connect into a percolating network with increasing concentration during the drying process at the surface.

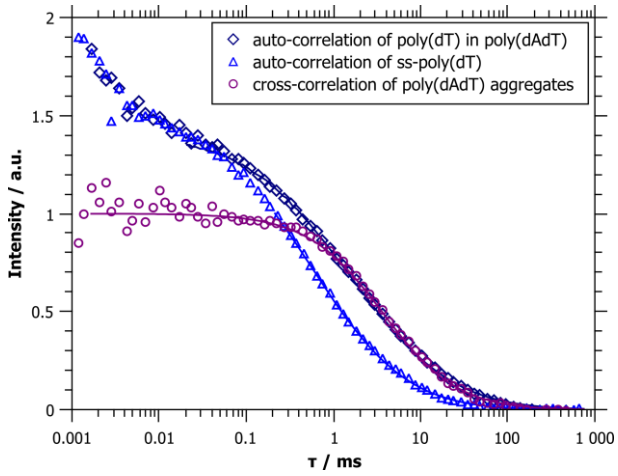

Figure 4. Auto-correlation functions of poly(dT) in poly(dAdT) aggregates and of the free ss-poly(dT) chains compared to the cross-correlation function of a mixed sample, showing that mixed samples contain much larger aggregates in addition to free ssDNA.

The aggregate formation in dilute solution becomes even more visible when considering the auto-correlation function of only one of the dyes in the mixed sample. In contrast to the cross-correlation function of both dyes, the auto-correlation shows the movement of only one dye, independent of the other. Figure 4 shows a bimodal decay in this auto-correlation function, which is consistent with the motion of some rather freely moving ssDNA chains and ssDNA chains confined within the larger poly(dAdT) aggregates, as observed by the cross-correlation of both dyes in the mixed sample (see Table 1). This confirms our assertions that even below the overlap concentration, larger ssDNA-assemblies are already formed in

solution and that the network is not continuous, with some free ssDNA coexisting in the mixture. A quantitative comparison of the amplitudes of the two modes in the auto-correlation function shows that about 54 % of the ssDNA are bound in aggregates, while 46 % behave like freely diffusing single strands (see Table S1). We cannot draw any detailed conclusions regarding the dynamics of ssDNA binding or leaving the DNA assemblies. However, since we can see two different movements of ssDNA in our samples, it is clear that such dynamics must be slower than the time scale of the FCS experiment, *i.e.*, dynamic exchanges must be taking place on a time scale slower than ~10 ms.

Effect of Varying System Parameters

To gain further insight into the process of network formation, we tested the effects of ionic strength, ssDNA concentration, strand length, and mixing ratio of the two complementary ssDNA on the network formation in solution and on surfaces (the complete set of FCS/FCCS curves and AFM images is shown in Figure S10).

As discussed above, the addition of divalent cations ($MgCl_2$) is essential for network formation on mica surfaces, since both, the DNA backbone, and the mica surface, are negatively charged. To ensure sufficient DNA binding, the salt concentration needs to exceed a certain minimum (typically higher than 1 mM $MgCl_2$). The AFM images in Figure 5 show that if the salt concentration is below this threshold, a non-percolating DNA network structure results or even no DNA is bound to the mica surface (all AFM images are also shown enlarged in the SI, Figures S6-S8). No upper limit for ionic strength was detected, likely because excess salt was washed from the surface during sample preparation. In our experiments we added 8 mM $MgCl_2$ to be well above the minimum threshold concentration.

Surprisingly, we observed the formation of DNA complexes in solution even in absence of added salt (Figure 5). We surmise that a very small amount of salt remains in the samples after synthesis (the products were purified only by centrifugal filtration in columns), which is sufficient to screen the DNA backbones and to allow hydrogen bond formation. To check this notion, we dialyzed a set of ssDNA solutions after synthesis to remove all remaining salt. In this case we detected a cross-correlation function

in the mixed sample only after addition of 10 μM of NaCl (Figure S12), which is just at the monomer concentration of the nucleotides. This suggests that polynucleotide charges must be shielded at least such that one counterion (Na^+) is present per base. Increasing the ionic strength of the solution did not change the aggregate size in solution. Furthermore, we found that the ion valency (*i.e.*, divalent Mg^{2+} or monovalent Na^+) did not notably affect aggregate formation (see Figure S12 for NaCl samples). In general, we observed that poly(dAdT) aggregate formation in solution is much more robust than on surfaces and only very small salt concentrations (~ 10 μM) are required for successful network formation.

Working at the correct DNA concentration and in the correct mixing range of the two strands is essential for successful network formation on surfaces (Figure 6). The correct surface concentration depends on the amount of sample drop cast on the surface and the size of the mica substrate. The concentration has to be sufficiently high for the DNA to cover the whole mica chip but low enough to result in a single layer network. In our case the optimal sample preparation procedure was to drop 6 μL of a 9 nM mixed DNA solution (total concentration of ssDNA strands) onto a 10 mm diameter mica disc. For ssDNA strands of ~ 1000 B this translates to 0.14 nm of DNA strand per nm^2 of mica (which yields a minimum spacing of 7.1 nm assuming an ideal square-lattice of DNA strands). This spacing is a lower bound, because of the hybridization of the strands. As seen in the AFM images (Figure 6), if the solution concentration of the ssDNA is too high, large aggregates and phase separation will ensue, whereas if the concentration is too low, no connected network can be formed. For ssDNA strands of ~1000 B each, the overlap concentration on the mica surface under these conditions would be 0.2 nM of the initially applied solution (assuming fully stretched chains). Our AFM images show that the actual concentration needed for a continuous network to form is much higher, because sufficient overlap of the ssDNA is required for making hydrogen bonding effective.

Surprisingly, almost no concentration effect on the aggregate size was found in solution. One could expect that higher concentrations would lead to larger complexes, but apparently this is not the case. As shown in Figure 6, the FCS measurements yielded similar decay times for a very wide range of DNA concentrations (from 0.5 to 890 nM) and even some systematic decrease of the effective size of the observed

aggregates is seen (see inset in Figure 6). We interpret these observations as follows: larger mixed aggregates are present at all concentrations, but due to the small confocal volume of FCS, the total size of these aggregates cannot be detected *via* this method. Instead, what is captured by the slow decay of the cross-correlation functions are most likely inner-aggregate fluctuations, dependent on the effective mesh size within the network (although we cannot rule out that this is already the finite size of the complex aggregates observed). In other words, the network aggregates are expected to grow with increasing concentration, but their total size cannot be detected. Instead, we observe a slight decrease of the average mesh size with increasing concentration (inset Figure 6) which some compaction of the structure. We assume that the same process also occurs when the sample is deposited onto a surface and the solvent is evaporating. On surfaces we found mesh sizes of 30-70 nm, *i.e.*, somewhat smaller than in solution, but in accordance with the concentration dependent trend.

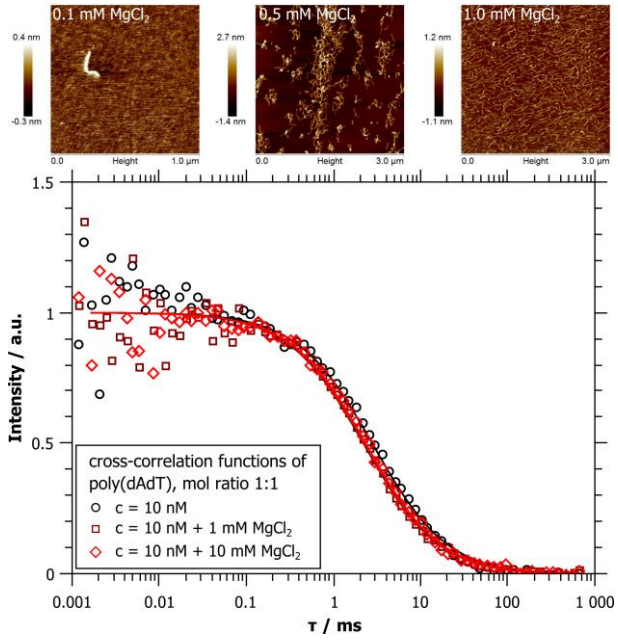

Figure 5. AFM images and cross-correlation functions from FCCS measurements of AT complexes (1000 B (poly(dA)) and 1300 B (poly(dT)) in a 1:1 molar ratio) at different amounts of added salt. All FCCS data was normalized to 1 for better comparison. Solid lines represent the best fit to the data. (Fit parameters can be found in the SI, AFM images are shown enlarged in Figure S6).

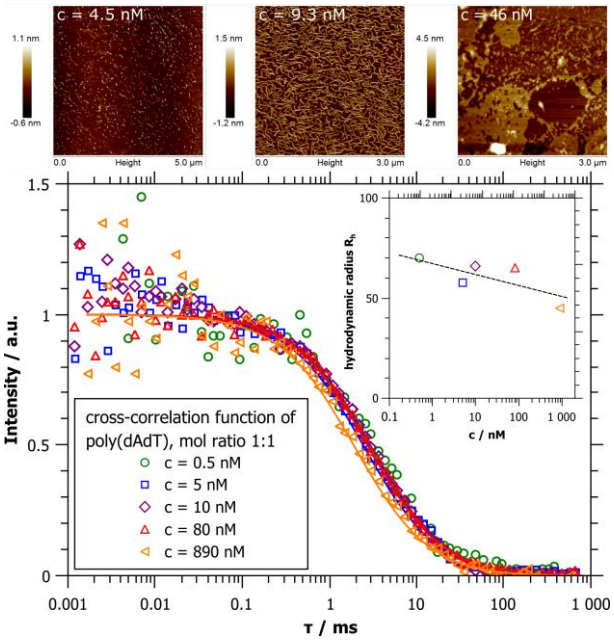

Figure 6. AFM images and cross-correlation functions from FCCS measurements of poly(dAdT) complexes (1000 B poly(dA) and 1300 B poly(dT) in a 1:1 molar ratio) at different total concentrations ranging from 0.5-890 nM with no added salt. All FCCS data was normalized to 1 for better comparison. Solid lines represent the best fit to the data, the dotted line in the inset is a guide for the eye only. (Fit parameters can be found in the SI, AFM images are shown enlarged in Figure S7).

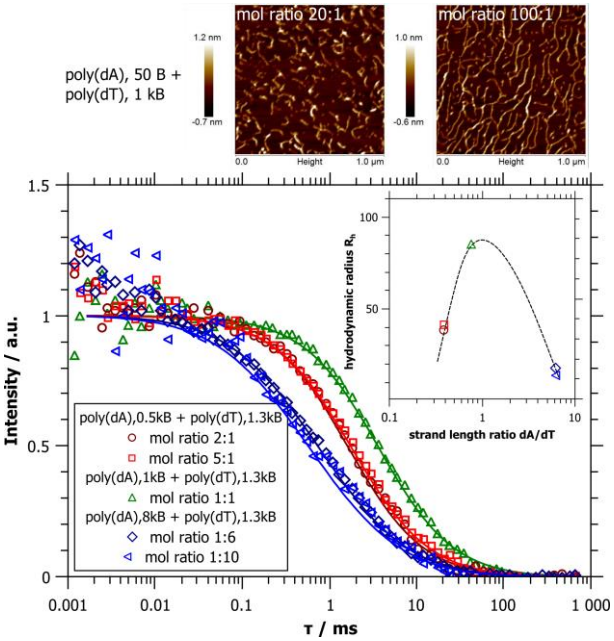

Figure 7. AFM images and cross-correlation functions from FCCS measurements of AT complexes (total concentration = 9 nM) obtained for different DNA strand lengths and mixing ratios. All FCCS data was

normalized to 1 for better comparison. Solid lines represent the best fit to the data, the dotted line in the inset is a guide for the eye only. (Fit parameters can be found in the SI, AFM images are shown enlarged in Figure S8).

Up to now we employed poly(dA) and poly(dT) strands of similar length (~ 1000 B) in a 1:1 molar ratio. However, enabled by our enzymatic polymerization synthesis route we can synthesize a wide range of strand lengths. To study the effect of different strand lengths on network formation, we employed poly(dA) of 50, 500, and 8000 bases mixed with poly(dT) of 1300 B fixed length. As seen in the AFM images in Figure 7 and S9, the strand length has a pronounced effect on network formation on surfaces. If the chain lengths of poly(dA) and poly(dT) differ substantially the resulting network structures appear discontinuous, even if the concentrations are adjusted to the nominal ratio (*i.e.*, equal numbers of bases). In this case, the concentration of short strands has to be increased much higher, to allow for the formation of percolating networks and uniform surface coverage. A similar effect was found in FCS/FCCS measurements in solution as well (Figure 7). Here, we employed poly(dT) of 500 or 8000 B together with poly(dT) of 1300 B. The use of shorter strands (or increasing length difference between strands of poly(dA) and poly(dT)) leads to smaller aggregates in solution. Varying the mixing ratio in solution has only a small effect on the size of the domains seen, in agreement with the notion that this is effectively related to the mesh size of the hybridized DNA. A marked maximum of aggregate size is observed when both strands are about the same length (see inset in Figure 7), which is consistent also with the AFM images shown in Figure S9.

CONCLUSIONS

We studied the aggregation behavior of mixtures of single stranded DNA (ssDNA) on surfaces and in dilute solution. While it is known that ss-poly(dA) and ss-poly(dT) easily self-assemble into large-scale networks when deposited onto a surface,[27] the precise dependence of the network structure on parameters like the strand length of the ssDNA, their mixing ratio, or their concentration was largely unclear. In particular, little has been known regarding the correspondence between network structures on surfaces and the solution

behavior prior to deposition. Surprisingly, we found that even in very dilute solution, i.e., well below the overlap concentration (~ [nM]), poly(dAdT) aggregates can form. This is borne out by FCCS measurements that showed significantly longer decay times for the FCCS correlation functions of mixed samples compared to those for free ssDNA. The hydrodynamic radius of 60-90 nm measured by FCS, can be understood to arise from fluctuations in the aggregates and is connected to their average network mesh size. Network mesh sizes depend on the relative concentrations and lengths of the polynucleotide chains. Additional experiments in which we varied the ionic strength, the total concentration, or the chain length, support these findings and prove that the aggregation process in dilute solution is quite robust and insensitive to changes in overall ssDNA concentration or ionic strength. While variation of the mixing ratio of ss-poly(dT) and ss-poly(dA) has little effect on the observed size in bulk solution, varying the relative strand lengths has a marked effect on aggregate size in solution, where a clear size maximum is obtained when equally long ss-poly(dT) and ss-poly(dA) are used.

When networks of ss-poly(dA) and ss-poly(dT) form on surfaces (by drop casting and subsequent solvent evaporation), their structure and mesh size roughly correlate with those of the aggregates in dilute solution. This is unexpected and suggests that surface networks are formed through the association of aggregates that are already present in dilute solution.

Our results, schematically summarized in Figure 8, are thus of importance for understanding and manipulating processes that lead to the formation of ssDNA networks on surfaces.

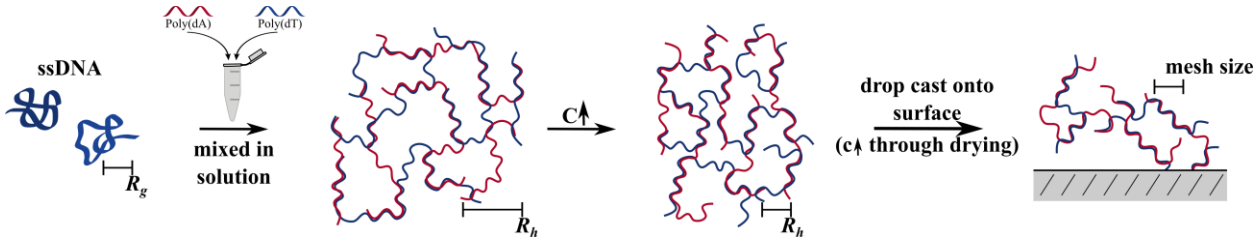

Figure 8. Schematic summarizing the results of the study. ss-poly(dA) and ss-poly(dT) spontaneously self-assemble into aggregates already in very diluted solutions, drying the solution on a surface results in extended 2D networks.

ASSOCIATED CONTENT

Supporting Information

Discussion of the overlap concentration. Supplementary AFM images of self-assembled DNA networks. Figures of the complete set of FCS and FCCS measurements. Complete set of fit parameters for all fitted FCS/FCCS measurements.

Author Contributions

M.S. performed the DNA synthesis and the experiments regarding the formation of DNA 2D-networks and AFM imaging, as well as FCS and FCCS experiments. A.P. contributed to the data analysis and evaluation of FCS and FCCS experiments. S.Z. and M.G directed the research and together with M.S. wrote the paper.

Notes

The authors declare no competing financial interest.

ACKNOWLEDGEMENTS

All authors thank Lei Tang for her continuous support for this project and especially her practical help and fruitful discussions regarding the DNA synthesis and AFM imaging. M. S. thanks the DAAD for funding the research stay in the USA via the PPP program (Projektkennziffer 57052141). The authors thank the International Research Training Group IRTG 1524 funded by the German Research Foundation (DFG) and the National Science Foundation (Research Triangle MRSEC DMR-1121107 and DMR-1411126) for financial support. The EU is thanked for funding the confocal microscope and its attached FCS unit through the EFRE program (EFRE 20072013 2/18).

REFERENCES

(1) Aherne, D.; Satti, A.; Fitzmaurice, D. Diameter-Dependent Evolution of Failure Current Density of Highly Conducting DNA-Templated Gold Nanowires. *Nanotechnology* **2007**, *18* (12), 125205. https://doi.org/10.1088/0957-4484/18/12/125205.

(2) Dukkipati, V. R.; Kim, J. H.; Pang, S. W.; Larson, R. G. Protein-Assisted Stretching and Immobilization of DNA Molecules in a Microchannel. *Nano Lett.* **2006**, *6* (11), 2499–2504. https://doi.org/10.1021/nl0617484.

(3) Amiram, M.; Quiroz, F. G.; Callahan, D. J.; Chilkoti, A. A Highly Parallel Method for Synthesizing DNA Repeats Enables the Discovery of Smart Protein Polymers. *Nat. Mater.* **2011**, *10* (2), 141–148. https://doi.org/10.1038/nmat2942.

(4) Tang, L.; Tjong, V.; Li, N.; Yingling, Y. G.; Chilkoti, A.; Zauscher, S. Enzymatic Polymerization of High Molecular Weight DNA Amphiphiles That Self-Assemble into Star-like Micelles. *Adv. Mater.* **2014**, *26* (19), 3050–3054. https://doi.org/10.1002/adma.201306049.

(5) Dey, S.; Fan, C.; Gothelf, K. v.; Li, J.; Lin, C.; Liu, L.; Liu, N.; Nijenhuis, M. A. D.; Saccà, B.; Simmel, F. C.; Yan, H.; Zhan, P. DNA Origami. *Nat. Rev. Methods Primers* **2021**, *1* (13), 1–24. https://doi.org/10.1038/s43586-020-00009-8.

(6) Tang, L.; Navarro, L. A.; Chilkoti, A.; Zauscher, S. High-Molecular-Weight Polynucleotides by Transferase-Catalyzed Living Chain-Growth Polycondensation. *Angew. Chem.* **2017**, *129* (24), 6882–6886. https://doi.org/10.1002/ange.201700991.

(7) Carneiro, K. M. M.; Aldaye, F. A.; Sleiman, H. F. Long-Range Assembly of DNA into Nanofibers and Highly Ordered Networks Using a Block Copolymer Approach. *J. Am. Chem. Soc.* **2010**, *132* (2), 679–685. https://doi.org/10.1021/ja907735m.

(8) Li, H.; Carter, J. D.; LaBean, T. H. Nanofabrication by DNA Self-Assembly. *Mater. Today* **2009**, *12* (5), 24–32. https://doi.org/10.1016/S1369-7021(09)70157-9.

(9) Becerril, H. A.; Woolley, A. T. DNA-Templated Nanofabrication. *Chem. Soc. Rev.* **2009**, *38* (2), 329–337. https://doi.org/10.1039/b718440a.

(10) Wang, R.; Zhang, G.; Liu, H. DNA-Templated Nanofabrication. *Curr. Opin. Colloid Interface Sci.* **2018**, *38*, 88–99. https://doi.org/10.1016/j.cocis.2018.09.006.

(11) Hui, L.; Zhang, Q.; Deng, W.; Liu, H. DNA-Based Nanofabrication: Pathway to Applications in Surface Engineering. *Small* **2019**, *15* (26), 1805428. https://doi.org/10.1002/smll.201805428.

(12) Gu, Q.; Cheng, C.; Gonela, R.; Suryanarayanan, S.; Anabathula, S.; Dai, K.; Haynie, D. T. DNA Nanowire Fabrication. *Nanotechnology* **2006**, *17* (1), R14–R25. https://doi.org/10.1088/0957-4484/17/1/R02.

(13) Condon, A. Designed DNA Molecules: Principles and Applications of Molecular Nanotechnology. *Nat. Rev. Genet.* **2006**, *7*, 565–575. https://doi.org/10.1142/9789814287005_0012.

(14) Alivisatos, A. P.; Johnsson, K. P.; Peng, X.; Wilson, T. E.; Loweth, C. J.; Bruchez, M. P.; Schultz, P. G. Organization of "nanocrystal Molecules" Using DNA. *Nature* **1996**, *382* (6592), 609–611. https://doi.org/10.1038/382609a0.

(15) Mirkin, C. A.; Letsinger, R. L.; Mucic, R. C.; Storhoff, J. J. A DNA-Based Method for Rationally Assembling Nanoparticles into Macroscopic Materials. *Nature* **1996**, *382* (6592), 607–609. https://doi.org/10.1038/382607a0.

(16) Harnack, O.; Ford, W. E.; Yasuda, A.; Wessels, J. M. Tris(Hydroxymethyl)Phosphine-Capped Gold Particles Templated by DNA as Nanowire Precursors. *Nano Lett.* **2002**, *2* (9), 919–923. https://doi.org/10.1021/nl020259a.

(17) Gu, Q.; Cheng, C.; Haynie, D. T. Cobalt Metallization of DNA: Toward Magnetic Nanowires. *Nanotechnology* **2005**, *16* (8), 1358–1363. https://doi.org/10.1088/0957-4484/16/8/063.

(18) Nickels, P.; Dittmer, W. U.; Beyer, S.; Kotthaus, J. P.; Simmel, F. C. Polyaniline Nanowire Synthesis Templated by DNA. *Nanotechnology* **2004**, *15* (11), 1524–1529. https://doi.org/10.1088/0957-4484/15/11/026.

(19) Tjong, V.; Tang, L.; Zauscher, S.; Chilkoti, A. "Smart" DNA Interfaces. *Chem. Soc. Rev.* **2014**, *43* (5), 1612–1626. https://doi.org/10.1039/c3cs60331h.

(20) Esmail Nazari, Z.; Gurevich, L. Controlled Deposition and Combing of DNA across Lithographically Defined Patterns on Silicon. *Beilstein J. Nanotechnol.* **2013**, *4*, 72–76. https://doi.org/10.3762/bjnano.4.8.

(21) Petit, C. A. P.; Carbeck, J. D. Combing of Molecules in Microchannels (COMMIC): A Method for Micropatterning and Orienting Stretched Molecules of DNA on a Surface. *Nano Lett.* **2003**, *3* (8), 1141–1146. https://doi.org/10.1021/nl034341x.

(22) Klinov, D.; Atlasov, K.; Kotlyar, A.; Dwir, B.; Kapon, E. DNA Nanopositioning and Alignment by Electron-Beam-Induced Surface Chemical Patterning. *Nano Lett.* **2007**, *7* (12), 3583–3587. https://doi.org/10.1021/nl072177y.

(23) Yokota, H.; Sunwoo, J.; Sarikaya, M.; van den Engh, G.; Aebersold, R. Spin-Stretching of DNA and Protein Molecules for Detection by Fluorescence and Atomic Force Microscopy. *Anal. Chem.* **1999**, *71* (19), 4418–4422. https://doi.org/10.1021/ac9902695.

(24) Michalet, X. Dynamic Molecular Combing: Stretching the Whole Human Genome for High-Resolution Studies. *Science* **1997**, *277* (5331), 1518–1523. https://doi.org/10.1126/science.277.5331.1518.

(25) Johnston, A. P. R.; Read, E. S.; Caruso, F. DNA Multilayer Films on Planar and Colloidal Supports: Sequential Assembly of like-Charged Polyelectrolytes. *Nano Lett.* **2005**, *5* (5), 953–956. https://doi.org/10.1021/nl050608b.

(26) Deng, Z.; Mao, C. DNA-Templated Fabrication of 1D Parallel and 2D Crossed Metallic Nanowire Arrays. *Nano Lett.* **2003**, *3* (11), 1545–1548. https://doi.org/10.1021/nl034720q.

(27) Kanno, T.; Tanaka, H.; Miyoshi, N.; Kawai, T. A New Self-Fabrication of Large-Scale Deoxyribonucleic Acid Network on Mica Surfaces. *Jpn. J. Appl. Phys.* **2000**, *39* (Part 2, No. 4A), L269–L270. https://doi.org/10.1143/JJAP.39.L269.

(28) Kawano, S. Fractal Dimension Analysis in Self-Assembled Poly(DA)·poly(DT) DNA Network on Mica Surface. *JSME Int. J. B* **2005**, *48* (2), 191–195. https://doi.org/10.1299/JSMEB.48.191.

(29) Doi, K.; Takeuchi, H.; Nii, R.; Akamatsu, S.; Kakizaki, T.; Kawano, S. Self-Assembly of 50 Bp Poly(DA)·poly(DT) DNA on Highly Oriented Pyrolytic Graphite via Atomic Force Microscopy Observation and Molecular Dynamics Simulation. *J. Chem. Phys.* **2013**, *139* (8). https://doi.org/10.1063/1.4818595.

(30) Song, Y.; Li, Z.; Liu, Z.; Wei, G.; Wang, L.; Sun, L.; Guo, C.; Sun, Y.; Yang, T. A Novel Strategy to Construct a Flat-Lying DNA Monolayer on a Mica Surface. *J. Phys. Chem. B* **2006**, *110* (22), 10792–10798. https://doi.org/10.1021/jp0564344.

(31) Monserud, J. H.; Schwartz, D. K. Mechanisms of Surface-Mediated DNA Hybridization. *ACS Nano* **2014**, *8* (5), 4488–4499. https://doi.org/10.1021/nn4064874.

(32) Peterson, E. M.; Manhart, M. W.; Harris, J. M. Single-Molecule Fluorescence Imaging of Interfacial DNA Hybridization Kinetics at Selective Capture Surfaces. *Anal. Chem.* **2016**, *88* (2), 1345–1354. https://doi.org/10.1021/acs.analchem.5b03832.

(33) Nöll, T.; Schönherr, H.; Wesner, D.; Schopferer, M.; Paululat, T.; Nöll, G. Construction of Three-Dimensional DNA Hydrogels from Linear Building Blocks. *Angew. Chem.-Int. Ed.* **2014**, *53* (32), 8328–8332. https://doi.org/10.1002/ANIE.201402497.

(34) Roth, E.; Glick Azaria, A.; Girshevitz, O.; Bitler, A.; Garini, Y. Measuring the Conformation and Persistence Length of Single-Stranded DNA Using a DNA Origami Structure. *Nano Lett.* **2018**, *18* (11), 6703–6709. https://doi.org/10.1021/acs.nanolett.8b02093.

(35) Broersma, S. Viscous Force Constant for a Closed Cylinder. *J. Chem. Phys.* **1960**, *32* (6), 1632–1635. https://doi.org/10.1063/1.1730995.

(36) Newman, J.; Swinney, H. L.; Day, L. A. Hydrodynamic Properties and Structure of Fd Virus. *J. Mol. Biol.* **1977**, *116* (3), 593–603. https://doi.org/10.1016/0022-2836(77)90086-9.

(37) Sim, A. Y. L.; Lipfert, J.; Herschlag, D.; Doniach, S. Salt Dependence of the Radius of Gyration and Flexibility of Single-Stranded DNA in Solution Probed by Small-Angle x-Ray Scattering. *Phys. Rev. E* **2012**, *86* (2), 021901. https://doi.org/10.1103/PhysRevE.86.021901.

(38) Johnson, A. T.; Wiest, O. Structure and Dynamics of Poly(T) Single-Strand DNA: Implications toward CPD Formation. *J. Phys. Chem. B* **2007**, *111* (51), 14398–14404. https://doi.org/10.1021/jp076371k.

(39) Plumridge, A.; Andresen, K.; Pollack, L. Visualizing Disordered Single-Stranded RNA: Connecting Sequence, Structure, and Electrostatics. *J. Am. Chem. Soc.* **2020**, *142* (1), 109–119. https://doi.org/10.1021/jacs.9b04461.

(40) Bacia, K.; Schwille, P. Practical Guidelines for Dual-Color Fluorescence Cross-Correlation Spectroscopy. *Nat. Protoc.* **2007**, *2* (11), 2842–2856. https://doi.org/10.1038/nprot.2007.410.

ToC GRAPHIC